STUDY ON OPTIMIZATION OF AL6061 SPHERE SURFACE ROUGHNESS IN DIAMOND TURNING BASED ON CENTRAL COMPOSITE DESIGN MODEL AND GREY WOLF OPTIMIZER ALGORITHMS

NGHIÊN CỨU TỐI ƯU HÓA ĐỘ NHÁM BỀ MẶT CẦU AL6061 KHI TIỆN BẰNG MŨI DAO KIM CƯƠNG SỬ DỤNG MÔ HÌNH THIẾT KẾ TỔNG HỢP TRUNG TÂM VÀ THUẬT TOÁN TỐI ƯU HÓA ĐÀN SÓI XÁM

Le Thanh Binh, Duong Xuan Bien*, Ngo Viet Hung, Chu Anh My, Hoang Nghia Duc, Nguyen Kim Hung, Bui Kim Hoa

Advanced Technology Center, Le Quy Don Technical University, Ha Noi, Vietnam

*Corresponding author: duongxuanbien@lqdtu.edu.vn

(Received: November 29, 2024; Revised: Febuary 08, 2025; Accepted: Febuary 11, 2025)

DOI: 10.31130/ud-jst.2025.494E

Abstract - This paper presents optimization results of the Al6061 surface roughness in turning ultra-precision based on the central composite design method (CCD) and the grey wolf optimization algorithm (GWO). The experimental matrix is built with three independent variables including spindle speed, feed rate and depth of cut. With the experimental data, the roughness regression model is established. The ANOVA module is used to evaluate the quality of the regression model. The GWO algorithm is used to optimize the roughness within the range of pre-determined cutting conditions. The most reasonable cutting parameter set is found to ensure that the surface roughness of the Al6061 material reaches the smallest value. The influence of parameter pairs on the roughness is analyzed specifically. The research results are of great significance in improving the surface quality of Al6061 material in turning ultra-precision.

Key words - Single-Point Diamond Turning (SPDT); surface roughness; spherical surface; CCD; GWO.

Tóm tắt – Bài báo trình bày kết quả nghiên cứu tối ưu hóa độ nhám bề mặt cầu vật liệu Al6061 khi tiện siêu chính xác (SPDT) dựa trên phương pháp thiết kế tổng hợp trung tâm (CCD) và thuật toán tối ưu hóa đàn sói xám (GWO). Ma trận thực nghiệm được xây dựng với ba biến độc lập gồm tốc độ trục chính, tốc độ chạy dao và chiều sâu cắt. Với dữ liệu của các thí nghiệm, mô hình hồi quy độ nhám được thiết lập. Modul ANOVA được dùng để đánh giá chất lượng mô hình hồi quy. Thuật toán GWO được sử dụng để tối ưu hóa độ nhám trong phạm vi chế độ cắt được xác định từ trước. Bộ thông số cắt hợp lý nhất được tìm ra nhằm đảm bảo độ nhám mặt cầu đạt giá trị nhỏ nhất. Ảnh hưởng của các cặp thông số tới độ nhám được phân tích cụ thể. Kết quả nghiên cứu có ý nghĩa quan trọng trong việc nâng cao chất lượng bề mặt cầu vật liệu Al6061 khi tiện siêu chính xác.

Từ khóa – Tiện kim cương đơn điểm; độ nhám; mặt cầu; CCD; GWO

1. Introduction

In the field of ultra-precision machining, achieving a surface with the desired roughness is a critical requirement to enhance product quality and meet stringent technical standards for the operating conditions of specialized components such as optical lenses, lens molds, spherical joints, spherical reflective surfaces, and more. Single-Point Diamond Turning (SPDT) is an advanced machining method widely used to produce highly precise surfaces (in the nanometer scale) [1]. Diamond cutting tools are employed in SPDT to achieve nanometer-level surface finish with specific requirements such as nanometer-scale edge sharpness and excellent wear resistance, allowing for machining with extremely low dimensional accuracy and surface roughness [2].

SPDT is commonly applied to machine non-metallic materials (e.g., ZnSe, Ge, CaF_2, Si) or non-ferrous metals such as aluminum and copper. This technology meets the demands for manufacturing high-precision components, such as spherical surfaces for optical lenses [3], lens molds [4], aluminum mirrors [5], and laser guidance systems [6]. Nowadays, SPDT has become increasingly popular, particularly effective in machining spherical surfaces on aluminum materials like Al6061. Studies [7] have demonstrated the excellent machinability (including surface roughness) of Al6061 spherical mirror surfaces when altering vibration frequency branching during the SPDT process.

Surface roughness is a critical technical parameter, used to measure the surface's unevenness after machining [8]. Numerous studies have focused on the technical factors affecting surface roughness, employing various predictive models, including the Response Surface Methodology (RSM) [9], Artificial Neural Networks (ANN) [10], and Adaptive Neuro-Fuzzy Inference Systems (ANFIS) [11]. Additionally, various algorithms have been used as tools to solve single or multi-objective optimization problems based on specific input parameters and conditions. Frequently applied algorithms include Genetic Algorithms (GA) [12-14], swarm-based algorithms (PSO, ACO) [15-16], and the Grey Wolf Optimization (GWO) algorithm [17-21]. RSM and ANN modeling [9-10] were described using 27 experiments, where a first-order regression equation was developed to predict surface roughness. Furthermore, the GWO algorithm is widely used for optimizing parameters or

technological processes. In [17], the GWO model was utilized to optimize parameters such as temperature, friction coefficient, and screw rotation speed in twin-screw extrusion to minimize material loss due to wear. An improved GWO algorithm with reduced computational time, faster convergence, and higher accuracy was proposed in [18] to optimize the rolling parameters of raw materials. Additionally, the GWO algorithm has been applied for tool wear prediction in SVR [19], performance prediction for desalination plants [20], and two-dimensional modeling of direct metal deposition processes [21]. In addition, a study [22] proposed a Genetic Gray Wolf Optimizer (GGWO) algorithm, which combines the principles of Gray Wolf Optimizer (GWO) with genetic algorithm operators to optimize wind farm layout. Compared with other algorithms such as PSO, ABC ACO, GGWO shows improved energy yield, faster convergence, and better compliance with layout constraints. The hierarchical leadership structure and genetic operation of the algorithm enhance the exploration and exploitation capabilities, outperforming traditional optimization methods. In the study [23], Mehdi compared the GWO algorithm with many other optimization algorithms such as PSO, GA, HJ, or Hybrid Methods in the context of building energy optimization. The results have shown that GWO achieved a good balance between convergence speed and solution quality, surpassing many existing algorithms in building energy optimization. Consequently, the GWO algorithm has demonstrated its feasibility and effectiveness in optimization studies alongside other popular algorithms.

In SPDT, three technological parameters: spindle speed (n- rev/min), feed rate (F- mm/min), and depth of cut (ap- µm), have a direct and significant impact on the surface quality of the machined component. Taper-cutting experiments [24] were applied to determine the transition depth between ductile and brittle regimes during SPDT machining of ZnSe spherical surfaces. The results indicated that reducing the feed rate (F) could achieve optimal surface roughness without introducing surface defects.

In this study, a regression model was developed to describe the relationship between the three SPDT parameters and the surface roughness of Al6061 spherical surfaces, based on the Central Composite Design (CCD) experimental method. Accordingly, the optimal roughness and the most suitable technological parameters were identified using the Grey Wolf Optimization (GWO) algorithm. The influence of parameter pairs on surface roughness was visually investigated, serving as a foundation for effective SPDT process control in the future for Al6061 spherical surfaces, contributing to improving the surface quality of ultra-precision products.

2. Research contents

2.1. Experimental design using the CCD model

2.1.1. Experimental model design

The primary objective of the experimental process is to collect data on the surface roughness of spherical surfaces corresponding to the technological parameters of different machining conditions. The entire machining process for the spherical surface of the Al6061 alloy workpiece was conducted on the ultra-precision lathe Nanoform® X (Figure 1) using a diamond cutting tool NN60R0635m WGC-MS0454 (Figure 4). The Al6061 workpiece (Figure 3) has the following geometric dimensions: height h = 20 mm, outer diameter $Ø$ = 30 mm, and spherical radius R = 19.5 mm. The specifications of diamond-cutting tool are presented in Table 1.

Figure 1. *Nanoform® X ultra-precision turning system*

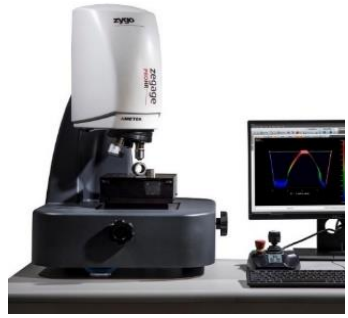

Figure 2. *The 3D optical profiler ZEGAGE PRO HR*

Figure 3. *Al6061 spherical surface*

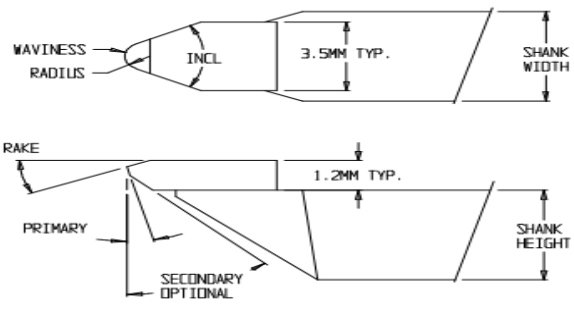

Figure 4. *Diamond cutting tool NN60R0635mWGC-MS0454*

Table 1. *Cutting tool specifications*

Specifications	Cutting edge radius	Rake angle	Cutting height	Primary Clearance	Included angle	Waviness
Dimensions	0.649 mm	-25°	7.475 mm	10°	60°	≤ 2 µm

Table 2. *Chemical compositions of Al6061*

Element	Mg	Si	Fe	Cu	Cr	Mn	Zn	Ti	Al
wt.%	0.99	0.55	0.33	0.20	0.12	0.10	0.08	0.03	Balance

The chemical compositions of Al6061 alloy [25] are presented in Table 2.

The SPDT process of the spherical surface of the Al6061 workpiece is illustrated in Figure 5. The workpiece is mounted on a vacuum chuck and machined using various cutting conditions within the experimental investigation range. A high-pressure water nozzle (machine mist) is employed to remove chips from the workpiece during the machining process, ensuring the safety and integrity of the spherical workpiece surface.

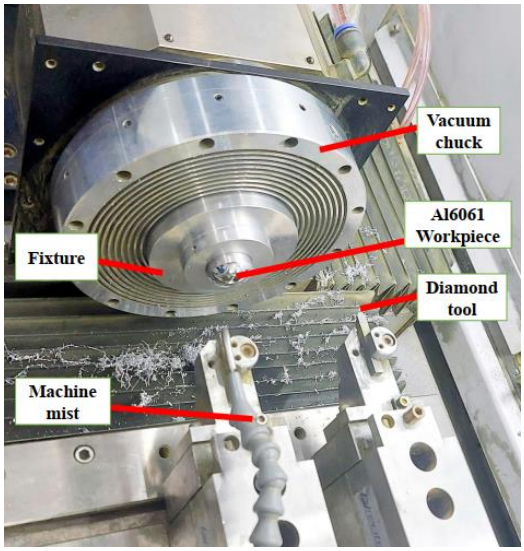

Figure 5. *Lathe system, fixtures, tools, and workpieces*

All measurements of surface roughness values after SPDT were performed on the 3D optical profiler ZEGAGE PRO HR (Figure 2). In this experiment, the workpieces were placed on a flat support. The optical lens with the camera was moved close to the position of the workpieces and the surface was scanned (Figure 6). The experimental surface roughness values summarized in Table 3 are the average results of two surface roughness measurements at two symmetrical positions on the spherical surface, corresponding to each set of technological parameters.

Figure 6. *Measurement on the 3D optical profiler ZEGAGE PRO HR*

Table 3. *Measurement results of the spherical surface roughness after machining*

No. Exp	n (rev/min)	F (mm/min)	ap (µm)	R_a (nm)
1	1000	5	2	5.606
2	2000	5	2	4.428
3	1000	25	2	4.218
4	2000	25	2	4.114
5	1000	5	8	2.233
6	2000	5	8	2.965
7	1000	25	8	6.131
8	2000	25	8	6.770
9	823.44	15	5	6.959
10	2176.56	15	5	4.345
11	1500	1.47	5	3.766
12	1500	28.53	5	5.480
13	1500	15	0.94	4.795
14	1500	15	9.06	7.228
15	1500	15	5	7.234
16	1500	15	5	6.820
17	1500	15	5	6.808

2.1.2. Central Composite Design (CCD) method

The Central Composite Design (CCD) method [26] is an experimental design technique widely used in research to construct experimental models, analyze data, and optimize processes. In this study, seventeen experiments measuring the surface roughness of spherical surfaces after SPDT were conducted, incorporating three technological parameters: depth of cut ap (µm), feed rate F (mm/min), and spindle speed n (rev/min). After performing SPDT according to the CCD experimental matrix and measuring the surface roughness R_a, data analysis and model construction were conducted. Statistical software DESIGN EXPERT was used to analyze the collected data. A quadratic regression model was developed to predict surface roughness based on the technological parameters.

The encoded factor matrix for the CCD experimental design with three factors and the corresponding ranges of technological parameters are presented in Table 4. In the CCD model, factors are assigned high levels (+1), low levels (-1), or central levels (0). Additionally, the central point spacing with orthogonal quadratic design $\alpha = 1.353$ was selected to ensure that the regression parameters (linear, interaction, and quadratic) are uncorrelated. This enhances the accuracy of data analysis and ensures precise evaluation of the regression model's suitability.

Table 4. *Technological parameter ranges*

Tech. Parameter	Corres. Variable	Low. (-1)	Cen. (0)	High (+1)
n (rev/min)	A	1000	1500	2000
F (mm/min)	B	5	15	25
ap (µm)	C	2	5	8

Figure 7 illustrates the distribution of experimental points in the CCD model. It can be observed that, with the number of experiments N = 17 and the number of

influencing factors k = 3, the experimental points are arranged around a cube, with three points located at the center. Six experiments represent axial points, whose distance from the cube is defined by the encoded value α = 1.353, and the remaining eight experimental points are distributed at the vertices of the cube.

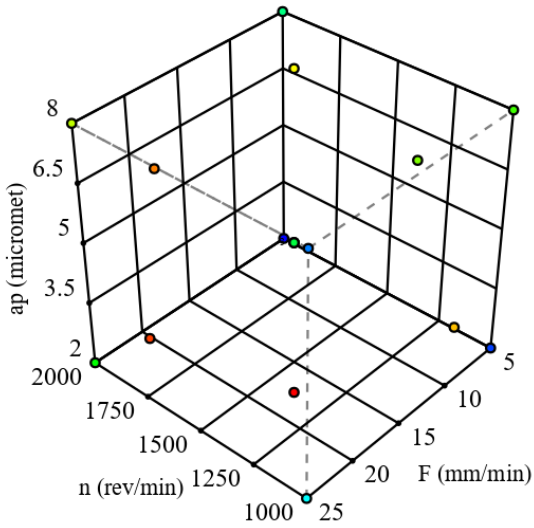

Figure 7. *Experimental distribution in the CCC model*

The specialized software DESIGN EXPERT was used to construct the regression equation based on the CCD experimental model with three input technological parameters. Figure 8 demonstrates the high reliability of the regression model. The coefficient of determination R^2 [27] is 0.8754, indicating a strong fit between the model and the experimental data. Furthermore, an Adeq Precision value greater than four 4 indicates that the model is adequate for navigating the design space.

Std. Dev.	0.8383	**R^2**	0.875
Mean	5.29	**Adjusted R^2**	0.7152
C.V. %	15.85	**Predicted R^2**	0.0080
		Adeq Precision	6.376

Figure 8. *Analysis of model fit with experimental data*

Source	Sum of Squares	df	Mean Square	F-value	p-value	
Model	34.57	9	3.84	5.47	0.0178	significant
A-n	1.02	1	1.02	1.45	0.2673	
B-F	5.94	1	5.94	8.45	0.0226	
C-t	0.7847	1	0.7847	1.12	0.3257	
AB	0.1203	1	0.1203	0.1712	0.6914	
AC	0.8791	1	0.8791	1.25	0.3003	
BC	11.05	1	11.05	15.73	0.0054	
A^2	3.03	1	3.03	4.31	0.0764	
B^2	10.22	1	10.22	14.54	0.0066	
C^2	1.52	1	1.52	2.16	0.1848	
Residual	4.92	7	0.7028			
Lack of Fit	4.80	5	0.9604	16.36	0.0586	not significant
Pure Error	0.1174	2	0.0587			
Cor Total	39.49	16				

Ra	=
+6.92	
-0.2958	* A
+0.7133	* B
+0.2594	* C
+0.1226	* AB
+0.3315	* AC
+1.18	* BC
-0.6724	* A^2
-1.23	* B^2
-0.4762	* C^2

Figure 9. *Results of ANOVA analysis and regression coefficients*

Figure 9 illustrates the ANOVA analysis results and the coefficients of the regression equation. At a significance level *p-value* < 0.05, the selected terms are x_2, x_2x_3, x_1^2, x_2^2. The term x_1^2 with *p-value* = 0.0764 < 0.1 belongs to the range of significance values and can be used to describe the effect of spindle speed on surface roughness. Consequently, the regression equation for surface roughness (R_a - nm) in terms of coded variables is determined as follows:

$$R_a = 6.92 + 0.7135x_2 + 1.18x_2x_3 - 0.6724x_1^2 - 1.23x_2^2 \quad (1)$$

The surface roughness after UPT is significantly influenced by three technological parameters: spindle speed n (rev/min), feed rate F (mm/min), and depth of cut ap (µm). Figure 10 evaluates the effects of these parameters on surface roughness. The curvature of the graph reflects the rate of change in surface roughness with respect to each parameter, indicating whether the change is rapid or gradual.

It can be observed that the surface roughness value R_a (nm) is minimally influenced by spindle speed n (rev/min). However, feed rate F (mm/min) and depth of cut ap (µm) have a significant impact on surface roughness. Specifically, roughness increases with an increase in feed rate F and decreases with an increase in depth of cut ap.

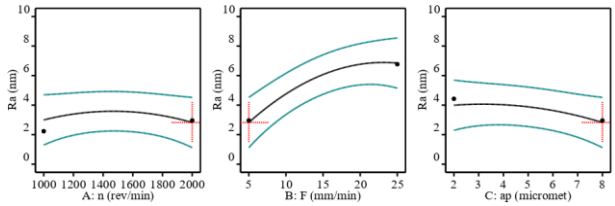

Figure 10. *Influence of parameters on surface roughness*

The above evaluations are qualitative assessments based on observations of the graph and the regression model. In fact, the technological parameters inherently interact with each other and collectively influence surface roughness. Moreover, experimental results are subject to external noise factors that affect the surface roughness measurements. Therefore, it is essential to design an optimization problem to confirm the relationship between surface roughness and the associated technological parameters.

2.2. Optimization design using GWO algorithm

2.2.1. Grey Wolf Optimization (GWO) algorithm

The Grey Wolf Optimization (GWO) algorithm, inspired by the predatory behavior of grey wolves, was introduced by Mirjalili et al. [28] and has been widely applied in various fields. In GWO, the grey wolf pack is classified into four main roles: Alpha (α), Beta (β), Delta (δ), Omega (ω). Each role contributes to the phases of encircling, attacking, and searching for prey within the search space to find the optimal solution.

The hunting process of grey wolves consists of three main phases: encircling, searching for prey, and attacking prey. In the GWO algorithm, these phases are modeled and integrated into its steps. The steps and conditions required to implement the GWO algorithm are shown in Figure 11.

Phase 1: Encircling Prey

The position of the wolves around the prey is adjusted using the following equations:

$$\vec{D} = \left| \vec{C}.\vec{X_P}(t) - \vec{X}(t) \right| \quad (2)$$

$$\overrightarrow{X}(t+1) = \overrightarrow{X_p}(t) - \overrightarrow{A}.\overrightarrow{D} \quad (3)$$

The coefficient vectors $\vec{A}$ and $\vec{C}$ calculated with vector $\vec{a}$ decreases linearly from 2 to 0 over iterations, and vector $\vec{r}$ are random vectors in [0, 1].

$$\vec{A} = 2.\vec{a}.\vec{r} - \vec{a}; \vec{C} = 2.\vec{r} \quad (4)$$

Phase 2: Searching for Prey

Grey wolves can identify the position of the prey and encircling it. The hunt is primarily guided by Alpha, with Beta and Delta providing support. The remaining wolves, known as Omega, update their positions based on the three leaders. The following equations illustrate this process:

$$\overrightarrow{D_\alpha} = \left|\overrightarrow{C_1}.\overrightarrow{X_\alpha} - \overrightarrow{X}\right|; \overrightarrow{D_\beta} = \left|\overrightarrow{C_2}.\overrightarrow{X_\beta} - \overrightarrow{X}\right| \quad (5)$$

$$\overrightarrow{D_\delta} = \left|\overrightarrow{C_3}.\overrightarrow{X_\delta} - \overrightarrow{X}\right|; \overrightarrow{X_1} = \overrightarrow{X_\alpha} - \overrightarrow{A_1}.(\overrightarrow{D_\alpha}) \quad (6)$$

$$\overrightarrow{X_2} = \overrightarrow{X_\beta} - \overrightarrow{A_2}.(\overrightarrow{D_\beta}); \overrightarrow{X_3} = \overrightarrow{X_\delta} - \overrightarrow{A_3}.(\overrightarrow{D_\delta}) \quad (7)$$

$$\overrightarrow{X}(t+1) = \frac{\overrightarrow{X_1} + \overrightarrow{X_2} + \overrightarrow{X_3}}{3} \quad (8)$$

Phase 3: Attacking Prey

When the distance between the wolves and the prey becomes sufficiently small, the wolves attack the prey. In the GWO algorithm, this process is simulated by reducing the value of the vector $\vec{a}$ from 2 to 0, thereby reducing the value of the vector $\vec{A}$ and narrowing the distance between the wolves and the prey.

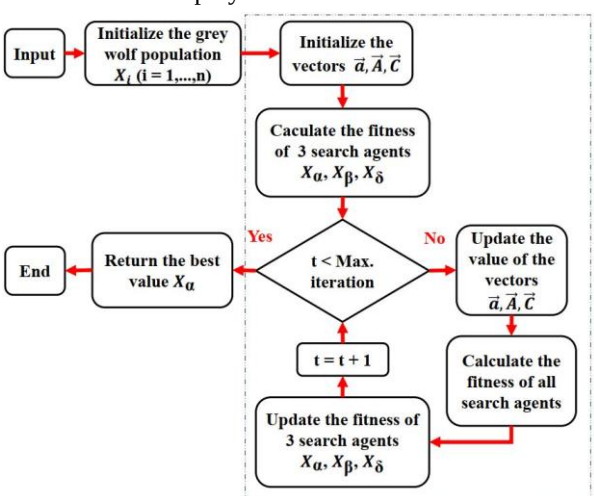

Figure 11. *Algorithm implementation steps in GWO*

2.2.2. Optimization results and discussion

The optimization problem for spherical surface roughness is considered, with the objective function derived from the established regression equation. The goal is to determine the optimal technological parameters to minimize the spherical surface roughness during machining.

The GWO algorithm was constructed under the conditions: $-1.353 < x_1, x_2, x_3 < +1.353$, corresponding to the technological parameter limits: $823.44 \le n \le 2176.56$ (rev/min); $1.47 \le F \le 28.53$ (mm/min); $0.94 \le ap \le 9.06$ (μm). The algorithm parameters are as follows: size population $S_A = 5$, maximum iterations $M_i = 100$.

The computational program was implemented using MATLAB. The optimization results are as follows: the optimal value was identified after the 8th iteration, achieving a surface roughness of R_a = 0.312 (nm) (Figure 12) with the encoded technological parameters: x_1 = 1.353, x_2 = -1.353, x_3 = 1.353, corresponding to the actual values: n = 2176.56 (rev/min), F = 1.47 (mm/min), ap = 9.06 (μm).

The dependence of the objective function on parameter pairs is presented in Figures 13, 14, and 15.

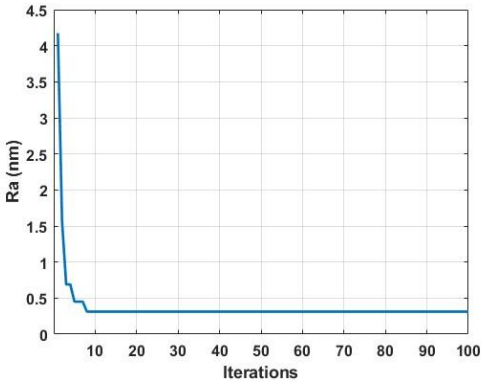

Figure 12. *The optimization value of surface roughness*

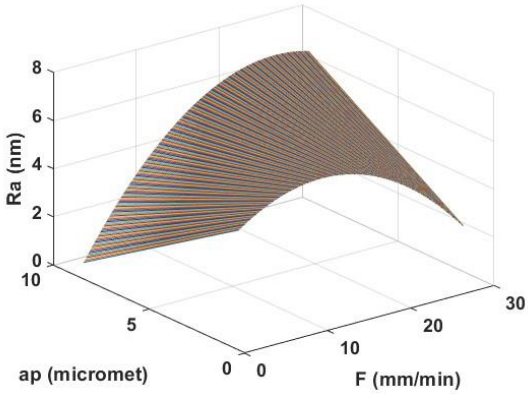

Figure 13. *Graph of the objective function* $R_a(ap, F)$

Figure 13 evaluates the influence of depth of cut (ap) and feed rate (F) on surface roughness. At the optimal spindle speed x_1=1.353 (n = 2176.56 (rev/min), the graph reveals that variations in feed rate (F) and depth of cut (ap) have a complex effect on surface roughness. When the feed rate (F) is fixed, the surface roughness value decreases linearly to a minimum point as the depth of cut (ap) increases. Conversely, when the depth of cut (ap) is fixed, increasing the feed rate (F) causes the surface roughness value to follow a parabolic curve, initially increasing to a maximum point before gradually decreasing. This indicates that the two parameters are interdependent and simultaneously affect surface roughness. In UPT, it is necessary to reduce the feed rate (F) while increasing the depth of cut (ap) to achieve optimal surface roughness value.

The dependence of surface roughness on spindle speed (n) and feed rate (F) is shown in Figure 14. At the optimal

depth of cut x_3=1.353 (ap = 9.06 µm), the surface roughness value changes along a quadratic curve as the spindle speed and feed rate. Therefore, the minimum surface roughness can be achieved by reducing both the spindle speed and feed rate within the considered range.

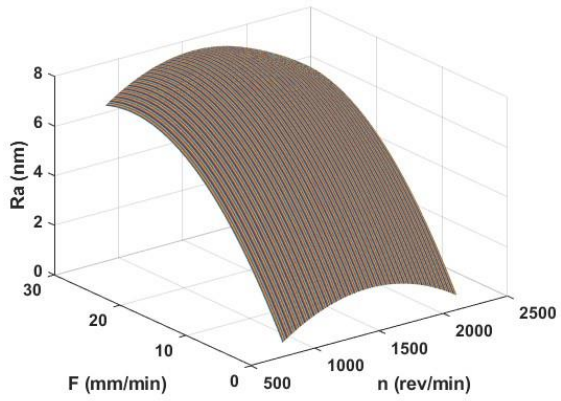

Figure 14. *Graph of the objective function* $R_a(F, n)$

Similarly, in Figure 15, the surface roughness reaches its minimum value when the spindle speed (n) is decreased and the depth of cut (ap). Increasing the spindle speed causes surface roughness to follow a quadratic curve while decreasing the depth of cut leads to a linear increase in surface roughness.

Similarly, in Figure 15, the surface roughness reaches its minimum value when the spindle speed (n) is decreased and the depth of cut (ap). Increasing the spindle speed causes surface roughness to follow a quadratic curve while decreasing the depth of cut leads to a linear increase in surface roughness.

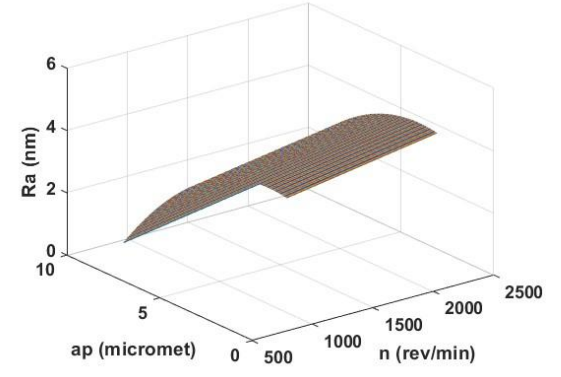

Figure 15. *Graph of the objective function* $R_a(ap, n)$

With the selected optimal technological parameters: n = 2177 (rev/min), F = 1.5 (mm/min), ap = 9 (µm), an experiment involving the SPDT of a spherical surface and measurements of surface roughness were conducted (Figure 16). The results from three measurements of the experimental surface roughness values R_a^{exp} are presented in Table 5. Comparing these values with the optimal roughness value obtained from the GWO algorithm $R_a^{pred} = 0.312$ (nm) reveals that the percentage error between the predicted and experimental values is allowable (1-2%), demonstrating the high accuracy of the predictive model.

Table 5. *Experimental results of the optimal parameter set*

No.exp	R_a^{exp} (nm)	R_a^{pred} (nm)	Error (%)
1	0.318	0.312	1.88
2	0.316	0.312	1.26
3	0.315	0.312	0.95

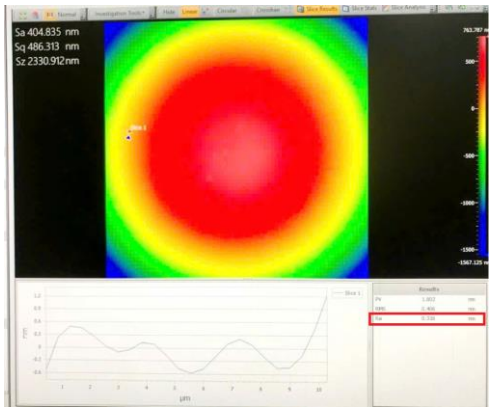

Figure 16. *Ra value with optimal parameter set*

3. Conclusions

Overall, the modeling problem using the CCD method and optimization using the GWO algorithm for surface roughness of Al6061 spherical surfaces in SPDT machining has been described and detailed. The CCD experimental model, based on 17 experimental results of surface roughness measurements, was used to construct a quadratic regression equation, providing input data for the GWO optimization algorithm. The evaluation results, through the R^2 criterion, demonstrate the high accuracy and reliability of the regression model with a sufficiently large number of experiments. The optimized surface roughness value R_a = 0.312 nm and the corresponding technological parameter (n = 2177 rev/min; F = 1.5 mm/min; ap = 9 µm) were determined using the GWO algorithm. Furthermore, the influence of parameter pairs was analyzed and evaluated in detail. Some key findings can be summarized as follows:

- The GWO algorithm develops a highly generalized model that effectively captures the complex relationships between technological parameters and the impact of parameter pairs on the optimal surface roughness value.

- Based on the coefficients of the regression model, the feed rate (F) has the most significant influence on surface roughness among the three parameters considered.

- The depth of cut (ap) has a greater effect on surface roughness than spindle speed (n).

The spherical surface roughness in SPDT is simultaneously influenced by all three technological parameters. The interactions between these factors affect surface roughness and overall surface quality. Within the investigation range, achieving optimal surface roughness and ensuring the best surface quality requires simultaneously reducing spindle speed (n), increasing depth of cut (ap), and finally reducing feed rate (F).

These findings are crucial for selecting appropriate technological parameters in terms of priority and value

when applying the SPDT method. Furthermore, the surface roughness value obtained from the SPDT experiment of the spherical surface using the optimal technological parameters further reinforces the validity of the conclusion and demonstrates the feasibility of the GWO algorithm. This is an effective solution for solving single-objective optimization problems, showing efficiency in establishing optimal solutions. It identifies a set of technological parameters that achieve the minimum surface roughness value, making it a promising choice for similar optimization studies in the future.

Acknowledgments: This research is funded by Vietnam National Foundation for Science and Technology Development (NAFOSTED) under grant number 107.01-2020.15.

Duong Xuan Bien and Chu Anh My participated in coming up with writing ideas and reviewing the article.

Ngo Viet Hung collected the data and wrote the manuscript.

Le Thanh Binh and Nguyen Kim Hung contributed to experimental design and data processing.

Bui Kim Hoa and Hoang Nghia Duc contributed to the interpretation of experimental data.

REFERENCES

[1] S. R. Chopade and S. B. Barve, "A single point diamond turning and integrated sensory system in nano machining: A survey, research issues, and challenges", *Materials Today: Proceedings* vol. 103, pp. 401-409, 2024.

[2] A. Gupta, A. Saini, N. Khatri, and A. Juyal, "Review of single-point diamond turning process on IR optical materials", *Materials Today: Proceedings*, vol. 69, pp. 435–440, 2022.

[3] Y. Dai, J. Jiang, G. Zhang, and T. Luo, "Forced-based tool deviation induced form error identification in single-point diamond turning of optical spherical surfaces", *Precision Engineering*, vol. 72, pp. 83–94, 2021.

[4] C. Shu, S. Yin, and S. Huang, "Preparation and performance of Ti/Ti-DLC composite coatings for precision glass molding", *Ceramics International*, vol. 50, no. 3, pp. 5210–5223, 2024.

[5] Y. Fu, S. Huang, Y. Yi, H. He, and J. Mao, "Mechanism of the effect of plastic deformation at different temperatures on the surface roughness of machined aluminum mirrors", *Materials and Design*, vol. 239, 2024.

[6] H. Liao, H. Ishihara, H. H. Tran, K. Masamune, I. Sakuma, and T. Dohi, "Precision-guided surgical navigation system using laser guidance and 3D autostereoscopic image overlay", *Computerized Medical Imaging and Graphics*, vol. 34, no. 1, pp. 46–54, 2010.

[7] G. Zhuang, W. Zong, and Y. Tang, "Statistical analysis and suppression of vibration frequency bifurcation in diamond turning of Al 6061 mirror", *Mechanical Systems and Signal Processing*, vol. 198, 110421, 2023.

[8] N. R. Sakthivel, J. Cherian, B. B. Nair, A. Sahasransu, L. N. V. P. Aratipamula, and S. A. Gupta, "An acoustic dataset for surface roughness estimation in milling process", *Data in Brief*, vol. 111108, 2024.

[9] S. T. Alam, A. N. M. A. Tomal, and M. K. Nayeem, "High-Speed Machining of Ti–6Al–4V: RSM-GA based Optimization of Surface Roughness and MRR", *Results in Engineering*, vol. 17, 100873, 2023.

[10] V. N. Malleswari, G. K. Manaswy, and P. G. Pragvamsa, "Prediction of surface roughness for fused deposition in fabricated work pieces by RSM and ANN technique", *Materials Today: Proceedings*, 2023.

[11] R. Kumar and N. R. J. Hynes, "Prediction and optimization of surface roughness in thermal drilling using integrated ANFIS and GA approach", *Engineering Science and Technology, an International Journal*, vol. 23, no. 1, pp. 30–41, 2020.

[12] K. S. Sangwan, S. Saxena, and G. Kant, "Optimization of machining parameters to minimize surface roughness using integrated ANN-GA approach", *Procedia CIRP*, vol. 29, pp. 305–310, 2015.

[13] V. Poonia, R. Kumar, R. Kulshrestha, and K. S. Sangwan, "Optimization of specific energy, scrap, and surface roughness in 3D printing using integrated ANN-GA approach", *Procedia CIRP*, vol. 116, pp. 324–329, 2023.

[14] V. Gopan, K. L. D. Wins, and A. Surendran, "Integrated ANN-GA approach for predictive modeling and optimization of grinding parameters with surface roughness as the response", *Materials Today: Proceedings*, vol. 5, no. 5, pp. 12133–12141, 2018.

[15] K. N. Babu, R. Karthikeyan, and A. Punitha, "An integrated ANN – PSO approach to optimize the material removal rate and surface roughness of wire cut EDM on INCONEL 750", *Materials Today: Proceedings*, vol. 19, pp. 501–505, 2019.

[16] A. Chetry, S. S. Phalke, and A. Nandy, "Achieving high precision and productivity in laser machining of Ti6Al4V alloy: A comprehensive study using a n-predictor polynomial regression model and PSO algorithm", *International Journal of Lightweight Materials and Manufacture*, vol. 8, pp. 127-140, 2025.

[17] P. Vasanthkumar, R. Balasundaram, and N. Senthilkumar, "Sliding-friction wear of a seashell particulate reinforced polymer matrix composite: modeling and optimization through RSM and Grey Wolf optimizer", *Transactions of the Canadian Society for Mechanical Engineering*, vol. 46, no. 2, pp. 329–345, 2022.

[18] W. Lin, J. Wang, B. Ren, J. Yu, X. Wang, and T. Zhang, "Robust optimization of rolling parameters of coarse aggregates based on improved response surface method using satisfaction function method based on entropy and adaptive chaotic gray wolf optimization", *Construction and Building Materials*, vol. 316, 125839, 2022.

[19] J. Wang, H. Liu, X. Qi, Y. Wang, W. Ma, and S. Zhang, "Tool wear prediction based on SVR optimized by hybrid differential evolution and grey wolf optimization algorithms", *CIRP Journal of Manufacturing Science and Technology*, vol. 55, pp. 129–140, 2024.

[20] Y. Yang, C. Wang, S. Wang, Y. Xiao, Q. Ma, X. Tian, C. Zhou, and J. Li, "Performance prediction model for desalination plants using modified grey wolf optimizer based artificial neural network approach", *Desalination and Water Treatment*, vol. 319, 100411, 2024.

[21] A. R. Dhar, D. Gupta, S. S. Roy, A. K. Lohar, and N. Mandal, "Covariance matrix adapted grey wolf optimizer tuned extreme gradient boost for bi-directional modelling of direct metal deposition process", *Expert Systems with Applications*, vol. 199, 116971, 2022.

[22] M. A. Pinazo, "New genetic gray wolf optimizer with a random selective mutation for wind farm layout optimization", *Heliyon*, vol. 10, no. 23, 2024.

[23] M. Ghalambaz, R. Jalilzadeh Yengejeh, and A. H. Davami, "Building energy optimization using Grey Wolf Optimizer (GWO)", *Case Studies in Thermal Engineering*, vol. 27, 2021.

[24] R. Geng, X. Yang, Q. Xie, W. Zhang, J. Kang, Y. Liang, and R. Li, "Ultra-precision diamond turning of ZnSe ceramics: Surface integrity and ductile regime machining mechanism", *Infrared Physics and Technology*, vol. 115, 2021.

[25] Z. Liu, J. Bao, W. Hu, and H. Yan, "Microstructure, interfacial reaction behavior, and mechanical properties of Ti3AlC2 reinforced Al6061 composites", *Transactions of Nonferrous Metals Society of China*, vol. 34, no. 9, pp. 2756–2771, 2024.

[26] B. Sadhukhan, N. K. Mondal, and S. Chattoraj, "Optimisation using central composite design (CCD) and the desirability function for sorption of methylene blue from aqueous solution onto Lemna major", *Karbala International Journal of Modern Science*, vol. 2, no. 3, pp. 145–155, 2016.

[27] M. Babič, G. Lesiuk, D. Marinkovic, and M. Calì, "Evaluation of microstructural complex geometry of robot laser hardened materials through a genetic programming model", *Procedia Manufacturing*, vol. 55, pp. 253–259, 2021.

[28] S. Mirjalili, S. M. Mirjalili, and A. Lewis, "Grey Wolf Optimizer", *Advances in Engineering Software*, vol. 69, pp. 46–61, 2014.